Effect of the iodine atom position on the phosphorescence of BODIPY derivatives: a combined computational and experimental study

(Article begins on next page)

20 April 2024

Effect of the iodine atom position on the phosphorescence of BODIPY derivatives: a combined computational and experimental study

Elena Bassan, Yasi Dai, Daniele Fazzi, Andrea Gualandi, Pier Giorgio Cozzi, Fabrizia Negri, Paola Ceroni

Effect of the iodine atom position on the phosphorescence of BODIPY derivatives: a combined computational and experimental study

Elena Bassan,[a,#] Yasi Dai,[a,#] Daniele Fazzi,[b] Andrea Gualandi,[a] Pier Giorgio Cozzi,[a,*] Fabrizia Negri,[a,c,*] Paola Ceroni[a,*]

[a] *Department of Chemistry Giacomo Ciamician, University of Bologna, Italy*

[b] *Institut für Physikalische Chemie, Department für Chemie, Universität zu Köln, Greinstr. 4-6, D-50939 Köln,Germany*

[c] *INSTM, UdR Bologna, Via F. Selmi, 2, 40126, Bologna, Italy*

Keywords: phosphorescence, triplet state, DFT calculations, spin orbit coupling calculations, singlet oxygen

Abstract

A new BODIPY derivative (***o*-I-BDP**) containing an iodine atom in the *ortho* position of the *meso*-linked phenyl group was prepared. Photophysical and electrochemical properties of the molecule were compared to previously reported iodo BODIPY derivatives, as well as to the non-iodinated analog. While in the case of derivatives featuring iodine substituents in the BODIPY core, efficient population of the triplet state is accompanied by a substantial positive shift of the reduction potential compared to pristine BODIPY, ***o*-I-BDP** displays phosphorescence and simultaneously maintains the electrochemical properties of unsubstituted BODIPYs. A theoretical investigation was settled in order to analyze results and rationalize the influence of iodine position on electronic and photophysical properties, with the purpose of preparing a fully-organic phosphorescent BODIPY derivative. TDDFT and spin-orbit coupling calculations shed light on the subtle effects played by the introduction of iodine atom in different positions of BODIPY.

1. Introduction

BODIPYs (*bo*ron-*dipy*rromethenes) are a class of organoboron compounds that has long received much attention for their high molar absorption coefficients, high fluorescence quantum yields and photostability. These properties have consequently led to a variety of applications, such as sensors for metal ions[1], fluorescent probes or labels targeted towards biological components[2].

The ease of their chemical modification has brought forth the development of derivatives that possess novel photophysical features. In particular, BODIPYs that efficiently populate their lowest triplet excited state[3] have been recently designed by three main strategies: (i) halogenation of the dye skeleton, (ii) coupling of BODIPY to electron donating chromophores in donor-acceptor dyads; (iii) BODIPY dimers. In the last two classes, population of the T_1 excited state is usually mediated by a photoinduced charge-transfer process and requires the synthesis of quite complex systems, while halogenation is an easier approach and affects the rate of spin-forbidden radiative and non-radiative processes. For instance, when iodine atoms are introduced at the 2 and 6

[#] The first two authors contributed equally to this work.

positions (Figure 1) intersystem crossing (ISC) becomes efficient and the lowest triplet state can be populated, as demonstrated by Nagano et al. in 2005[4]. This non-radiative deactivation becomes faster thanks to the internal heavy atom effect, as commonly observed for metal complexes containing heavy metal ion, e.g. Ru(II) or Ir(III) complexes[5]. Halogenation of the BODIPY core has therefore been extensively investigated for the development of drugs in photodynamic therapy[6], as it enables the production of cytotoxic singlet oxygen without the use of heavy metals. More recently, these derivatives have been used as photosensitizers in photocatalytic reactions[7], which has required taking into consideration the effect of halogenation on their electrochemical redox potentials as well.

This work focuses on a series of iodinated BODIPY derivatives (Figure 1*Figure 1*) and the rationalization of the effect that the position of the iodine atom has on the photophysical and electrochemical properties of such compounds. **I₂-BDP** is characterized by the presence of two iodine atoms directly linked to the chromophoric unit, while **p-I-BDP** possesses one iodine atom in the *para* position of the *meso*-linked phenyl group. The new BODIPY derivative, **o-I-BDP**, was designed by placing one iodine atom in the *ortho* position of the phenyl group so that the halogen is placed close to the BODIPY core but is not directly attached to it. The effect of this substitution was studied photophysically, electrochemically and computationally.
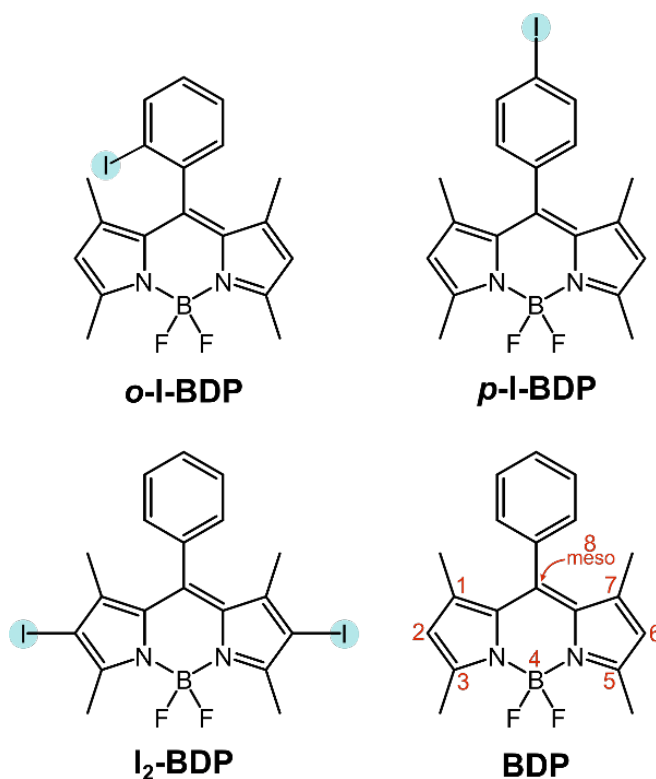
Figure 1. Structure of the studied compounds and IUPAC numeration.

2. Experimental and computational details

2.1 Synthesis of compounds

2-iodobenzaldehyde[8], **p-I-BDP**[9] and **I₂-BDP**[10] were prepared according to literature procedures.

Synthesis of *o*-I-BDP. Dipyrromethane was synthesized according to a modified literature procedure[11]. Deionized water (17 mL) was degassed in a Schlenk tube and 2-iodobenzaldehyde

3

(0.42 mmol, 97 mg, 1 eq.) was subsequently added. Distilled 2,4-dimethylpyrrole (10.5 mmol, 1.00 g, 25 eq.) was introduced, and the mixture was shielded from light and vigorously stirred at 80°C for 24 hours. After cooling at room temperature, AcOEt (20 mL) was added and the organic phase was separated. Aqueous phase was extracted with AcOEt (3 x 20 mL), and the collected organic phases were evaporated under reduced pressure to obtain a brown oil. The residue was filtrated on a silica plug (cyHex:DCM:AcOEt, 7:2:1), and the solvent was removed under reduced pressure to obtain dipyrromethane, that was employed in the next step without further purification. Dipyrromethane was dissolved in anhydrous DCM (25 mL) and 2,3-dichloro-5,6-dicyano-1,4-benzoquinone (DDQ) (0.5 mmol, 114 mg, 1.2 eq.) was added. After stirring at r.t. for 12 hours, anhydrous Et$_3$N (25.2 mmol, 2.55 g, 60 eq.) was added followed, after 30 minutes, by the addition of BF$_3$·Et$_2$O (16.8 mmol, 2.38 g, 40 eq.). The solution was stirred for one hour and then filtered through a pad of Celite washing with DCM. Deionized water (20 mL) was added to the filtrate and the organic phase was separated. Aqueous phase was extracted with DCM (3 x 20 mL), and the collected organic phases were evaporated under reduced pressure. *o*-**I-BDP** was purified by flash chromatography (cyHex:AcOEt, 4:1) to obtain an orange solid (37% yield). ^{1}H NMR: (CDCl$_3$, 400 MHz) δ 1.38 (s, 6H), 2.55 (s, 6H), 5.98 (s, 2H), 7.94 (d, 1H, J = 8.0 Hz), 7.48 (t, 1H, J = 7.6 Hz), 7.29 (d, 1H, J = 7.5 Hz), 7.15 (t, 1H, J = 7.7 Hz); ^{13}C NMR (CDCl$_3$, 100 MHz) δ 156.0, 142.4, 139.9, 139.6, 130.4, 129.0, 128.9, 121.2, 98.2, 14.7, 14.0; ^{19}F NMR (CDCl$_3$, 376.5 MHz) δ 145.93 (ddd, 1F, J = 32.9, 66.4, 109.4 Hz), 146.66 (ddd, 1F, J = 31.6, 64.4, 109.4 Hz).

2.2 Computational details

Ground state equilibrium structures of each molecule shown in *Figure 1* were determined with density functional theory (DFT) calculations. Two functionals were considered in this case, the B3LYP and the M06-2X. The 6-31G* basis set was used for all atoms except iodine for which the LANL2DZ basis set and pseudopotential[12] were employed. Solvent effects were included by means of the Polarizable Continuum Model (PCM)[13]. According to the experimental measurements, MeCN (ε=35.688) was considered as solvent. The corresponding calculations are labelled as PCM-B3LYP/6-31G*/LANL2DZ and PCM-M06-2X/6-31G*/LANL2DZ. The nature of the stationary points determined by geometry optimization were verified by vibrational frequency calculations carried out at the same level of theory. All the reported geometries correspond to minima.

Excited state wavefunctions and excitation energies were calculated with time-dependent (TD)-DFT, using the M06-2X functional and the 6-311G* basis set, while iodine atoms were described as indicated above. Due to the constrained cyanine nature of BODIPY and the insufficient electron correlation at TD-DFT level, excitation energies are systematically overestimated by ca. 0.4-0.5 eV[14–16] at this level of theory. Nevertheless, it has been shown in several benchmark works that the M06-2X functional is suitable to describe excitation energies in BODIPY derivatives and the variations induced by side groups, modifications of the skeleton, stiffening or extension of the conjugated path[16–19]. Excited state calculations are indicated as PCM-TD-M06-2X/6-311G*/LANL2DZ. Excitation energies in solution were initially determined with the use of the standard linear response (LR). Solute-solvent polarization effects in excited states were additionally determined with the state specific (SS) corrected linear response (cLR)[20,21] approach. Only the fast solvent component was equilibrated (hereafter indicated as NEQ) in calculations of excited state energies used to model absorption spectra, while a fully equilibrated solvent was assumed (hereafter labelled EQ) for excited state energies employed in the discussion of photo-deactivation processes. Accordingly, the solvent correction included in excited state calculations

is indicated by the label LR, cLR(NEQ) or cLR(EQ). All calculations were performed with the Gaussian 16 package.[22]

For spin-orbit coupling (SOC) calculations, we considered both PCM-B3LYP (*Figure S1* and *Table S1*) and PCM-M06-2X (*Figure S2* and *Table S2*) geometries. TD-M06-2X/6-31G* calculations (3-21G basis set was used for iodine atoms) were carried out with ORCA 4.2.1 package[23]. The SOC integrals were calculated with the spin-orbit mean-field (SOMF) method, with one-center approximation applied to the exchange term, (SOMF(1X))[24,25], the default choice of ORCA 4.2.1.

3. Results and discussion

3.1 Synthesis

The preparation of **o-I-BDP** was carried out with a slight modification of a synthetic procedure previously reported by one of us.[11] The synthesis takes advantage of the standard approach employed for BODIPY dyes. A dipyrromethane, obtained in a convenient green "on water" procedure starting from *o*-iodobenzaldehyde is oxidized with DDQ, and, without purification, the derivative is treated with BF_3 ether complex in the presence of an excess of base (Et_3N). Compared to other procedures published in the literature, the "on water" procedure is avoiding Lewis or Brønsted acids, limiting the formation of polypyrrolic by-products. The final BODIPY is conveniently purified by chromatography, in moderate isolated yields.

3.2 Photophysical characterization

The photophysical properties of **o-I-BDP** were studied in air-equilibrated acetonitrile solution and compared to those of **I_2-BDP**, **p-I-BDP** and **BDP** so as to rationalize the effects brought about by iodination at different sites of the BODIPY core. The absorption spectrum of **o-I-BDP** (Figure 2B, solid line) presents a narrow band that corresponds to the $S_0 \rightarrow S_1$ electronic transition ($\lambda_{max} = 503$ nm, $\varepsilon = 63600$ $M^{-1}cm^{-1}$). This band is blue-shifted compared to that of **I_2-BDP** and slightly red-shifted compared to that of **p-I-BDP** and **BDP**[26] (Table 1). The emission spectrum recorded at room temperature (Figure 2B, dashed line) peaks at 521 nm and is attributable to **o-I-BDP**'s fluorescence, given its small Stokes shift and its lifetime of 5.0 ns. The same trend observed for the absorption maxima is maintained for the fluorescence maxima as well (Table 1).

Interestingly, **o-I-BDP** presents a new emission band ($\lambda_{max} = 765$ nm) at 77K in an EtOH/MeOH (1:1 v/v) glassy matrix with a lifetime of 520 µs (Figure 2B, dotted line). This band is assigned to **o-I-BDP**'s phosphorescence due to its larger Stokes shift, its absence in aerated solutions at room temperature and its decay lifetime. **I_2-BDP** also presents a similar band in the same spectral region, whereas **p-I-BDP** does not (Figure 2A and C, and Table 1). These results are ascribable to the different positions occupied by iodine atoms, which strongly influence the efficiency of ISC between the lowest singlet (S_1) and triplet state (T_1), as well as the efficiency of phosphorescence. In fact, given the distance of the iodine atom from the chromophoric core, the ability of **p-I-BDP** to populate its lowest triplet state and thus display phosphorescence is strongly reduced and its photophysical properties resemble those of non-iodinated **BDP**[26,27]. Conversely, ISC is favored in **I_2-BDP** since the two iodine atoms are directly attached to the BODIPY skeleton. In the case of the **o-I-BDP** derivative, the presence of one iodine atom in the vicinity of the BODIPY core allows it to populate the lowest triplet excited state, even though it is not directly appended to it.
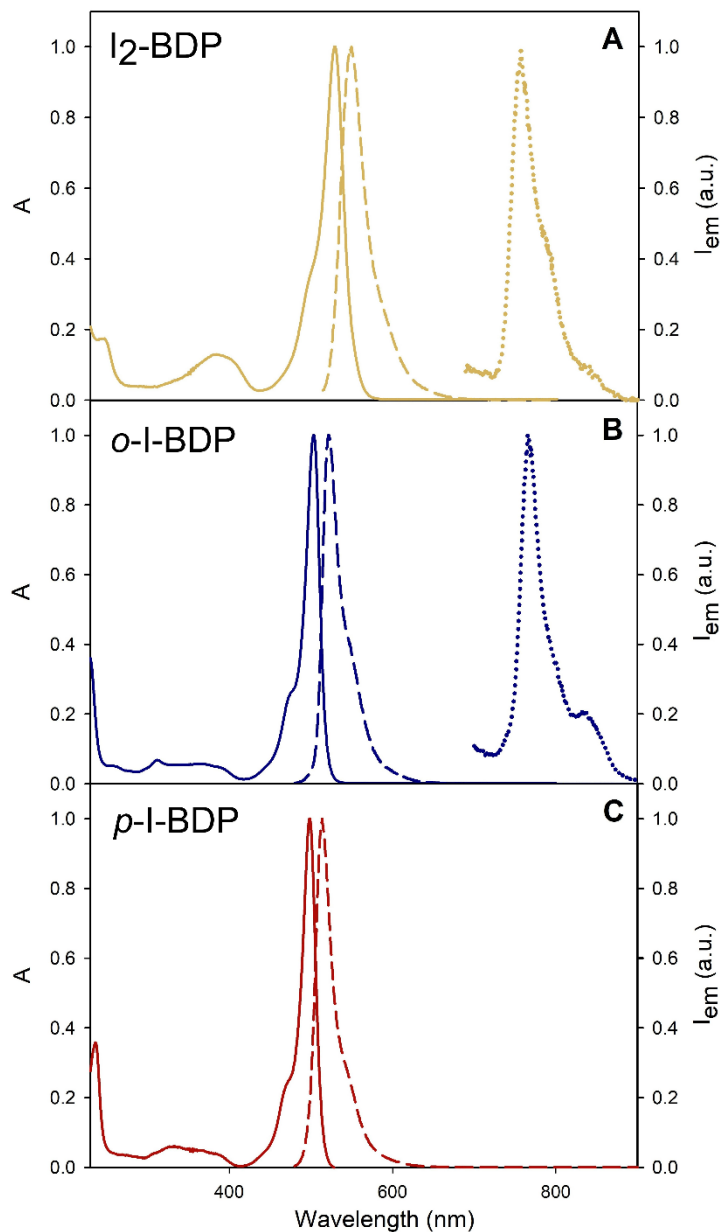
Figure 2. Absorption (solid line), fluorescence (dashed line), and phosphorescence (dotted line) spectra of **I₂-BDP** (A), ***o*-I-BDP** (B) and ***p*-I-BDP** (C).

In order to understand the extent of this deactivation pathway, fluorescence quantum yields (Φ_{FLUO}) and singlet oxygen quantum yields (Φ_Δ) were measured for the three compounds (Table 1) and compared to those of **BDP**. As schematically depicted in Figure 3, where competitive deactivation pathways are considered, fluorescence quantum yield is expected to decrease upon increasing the rate of ISC. Simultaneously, Φ_Δ is expected to increase because singlet oxygen is generated by energy transfer from the lowest triplet excited state (T_1) of the BODIPY. Φ_Δ is thus an indirect measurement of the efficiency of T_1 population according to the following equation:

$$\Phi_\Delta = \eta_{T_1} \times \eta_{ET} \tag{1}$$

6

where η_{T_1} is the efficiency of T_1 population and η_{ET} is the efficiency of the bimolecular energy transfer process between BODIPY and ground-state molecular oxygen.
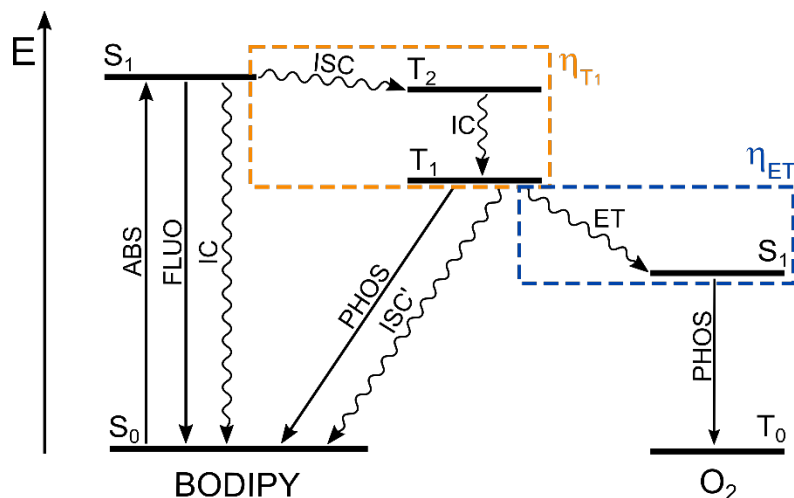

Figure 3 Jablonski diagram illustrating the main energy levels and deactivation pathways for BODIPY derivatives in the presence of molecular oxygen. The role of the T_2 state will be discussed in the computational section.

In accordance with literature data[28], **I$_2$-BDP** is characterized by the lowest value of Φ_{FLUO} and the highest value of Φ_Δ because the two iodine atoms are positioned in such a way that they are highly effective at inducing ISC and obtaining an efficient T_1 population. ***o*-I-BDP**'s Φ_{FLUO} (56%) is similar to that of ***p*-I-BDP** but, remarkably, Φ_Δ is 35% for ***o*-I-BDP** and not detectable for ***p*-I-BDP**. These results indicate that the location of the iodine atom is crucial for the population of the triplet state: ***o*-I-BDP** exhibits a quite efficient T_1 population, although not as efficient as in **I$_2$-BDP**. On the contrary, ***p*-I-BDP** is unable to undergo efficient ISC, similarly to what is reported for **BDP**[28]. Lastly, the higher Φ_{FLUO} of ***o*-I-BDP** compared to ***p*-I-BDP** can be imputed to the increased steric hindrance of its *meso* substituent. In fact, a substituent in the *ortho* position decreases its rotational freedom and, in turn, its non-radiative deactivation.

Table 1 Photophysical properties of studied compounds in air-equilibrated MeCN solution.

Molecule	$\lambda_{max\ ABS}$ (nm)	$\lambda_{max\ FLUO}$ (nm)	τ_{FLUO} (ns)	Φ_{FLUO}	$\lambda_{max\ PHOS}$ (nm)[a]	τ_{PHOS} (ms)[a]	Φ_Δ
***o*-I-BDP**	503	521	5.0	56%	765	0.52	35%
***p*-I-BDP**	498	514	3.3	45%	n.d.	/	n.d.
I$_2$-BDP	530	548	/[b]	1.8%	757	1.20	70%
BDP[26–28]	497	507	3.18	48%	/	/	1%[c]

3.3 Electrochemical characterization

The ground state electrochemical potentials of the three BODIPY derivatives were studied by means of cyclic voltammetry (Table 2). **o-I-BDP** shows chemically and electrochemically reversible electron transfer processes, both in the anodic (+1.20 V vs. SCE) and cathodic region (-1.10 V vs. SCE) (Figure 4, blue line).
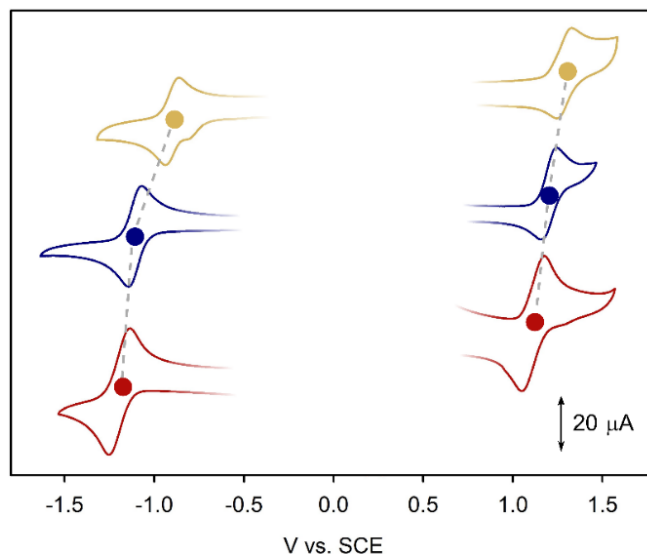

Figure 4. Cyclic voltammetry of **I$_2$-BDP** (yellow line), **o-I-BDP** (blue line) and **p-I-BDP** (red line) (0.5 mM) in degassed MeCN solution containing tetraethylammonium hexafluorophosphate 0.05 M, as the supporting electrolyte and ferrocene as the internal standard. Working electrode: glassy carbon; counter electrode: Pt wire; quasi-reference electrode: Ag wire; scan rate= 0.3 V/s. Ferrocene's peaks have been removed for clarity.

Both these redox potentials are negatively shifted compared to those of **I$_2$-BDP**, and are comparable to those measured for **p-I-BDP** and **BDP**[10], as presented in Figure 4. Indeed, the presence of halogen atoms directly connected to the BODIPY core reduces its electron density, while derivatizations present on the *meso*-linked phenyl group have little influence on the electrochemical properties thanks to its orthogonality with respect to the chromophoric unit. Therefore, iodination in the *ortho* position of the phenyl group allows to maintain the redox potentials typical of fluorescent BODIPYs meanwhile allowing the population of their lowest triplet excited state.

Table 2 Redox potentials of the studied compounds in MeCN in V vs. SCE.

Molecule	E(B/B$^{\cdot-}$) (V)	E(B$^{\cdot+}$/B) (V)
o-I-BDP	-1.10	+1.20
p-I-BDP	-1.12	+1.18
I$_2$-BDP	-0.90	+1.29
BDP[10]	-1.19	+1.21

3.4 Modeling photophysical properties of **BDP** and iodinated derivatives

To assist the interpretation of experimental results and rationalize the influence of Iodine position, a computational investigation on the electronic structure and photophysical properties was carried out on BODIPY derivatives shown in Figure 1.

3.4.1 Ground state structures and frontier molecular orbitals

The computed equilibrium structures and bond lengths of the four BODIPY derivatives are collected in *Figure S1* and *Figure S2*. We note that while PCM-B3LYP/6-31G*/LANL2DZ predicts an almost planar BODIPY core (the only exception is **I₂-BDP**) and an almost orthogonal phenyl moiety for all molecules (see *Figure S1* and *Table S1*), PCM-M06-2X/6-31G*/LANL2DZ geometries display deviations from orthogonality for the phenyl substituent, except for ***o*-I-BDP,** and are characterized by a more markedly out of plane tilted BF₂ group, as indicated by the dihedral angles in *Table S2*. In *Figure 5* and *Figure S4*, we see that the HOMO (H) and LUMO (L), calculated at both levels of theory, are localized on the BODIPY core. Focusing on the set of PCM-B3LYP molecular orbitals (MOs, *Figure 5*), we note that the shape of the H is the same for all molecules except for **I₂-BDP**. In the latter case significant electron density is computed also on the two iodine atoms. The electron density of L is almost the same across the four molecules but due to the electron withdrawing character of iodine and its substitution on the BODIPY core, the LUMO energy of **I₂-BDP** is significantly lowered. The substituent effect can be qualitatively explained via orbital interaction between fragments, or more quantitatively rationalized via absolutely localized molecular orbitals as demonstrated in recent work[29]. Due to the deviation from orthogonality, the MOs computed at PCM-M06-2X/6-31G*/LANL2DZ geometries (*Figure S4*), display some minor density contribution to phenyl substituents, especially for **I₂-BDP**.
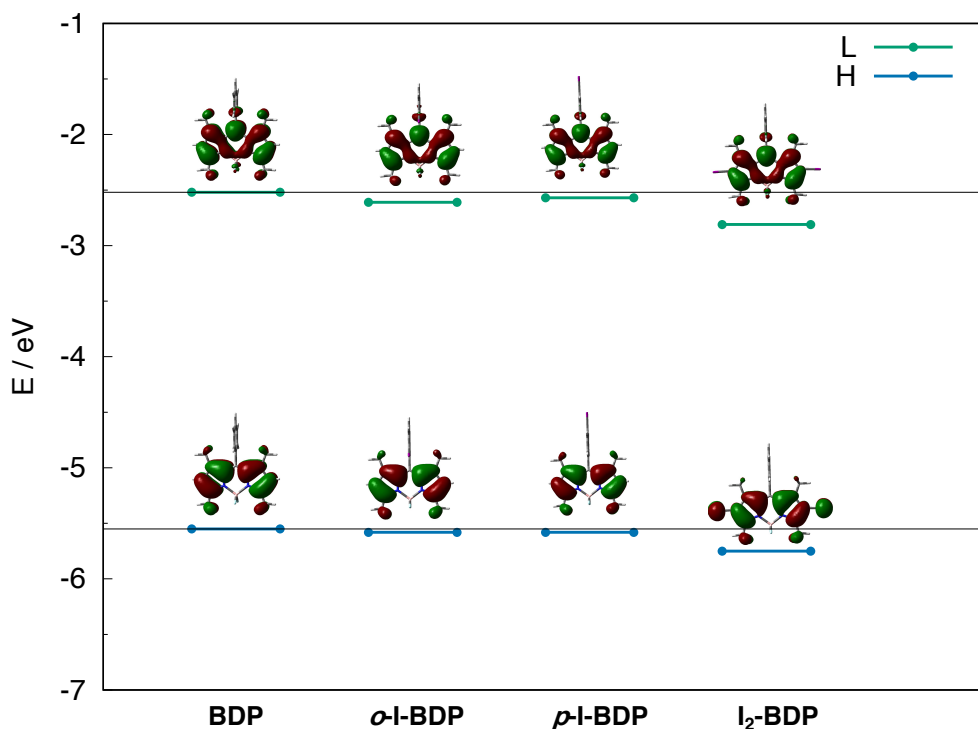

Figure 5. Shapes and energies of H and L of **BDP** and iodinated derivatives calculated at PCM-B3LYP/6-31G*/LANL2DZ level.
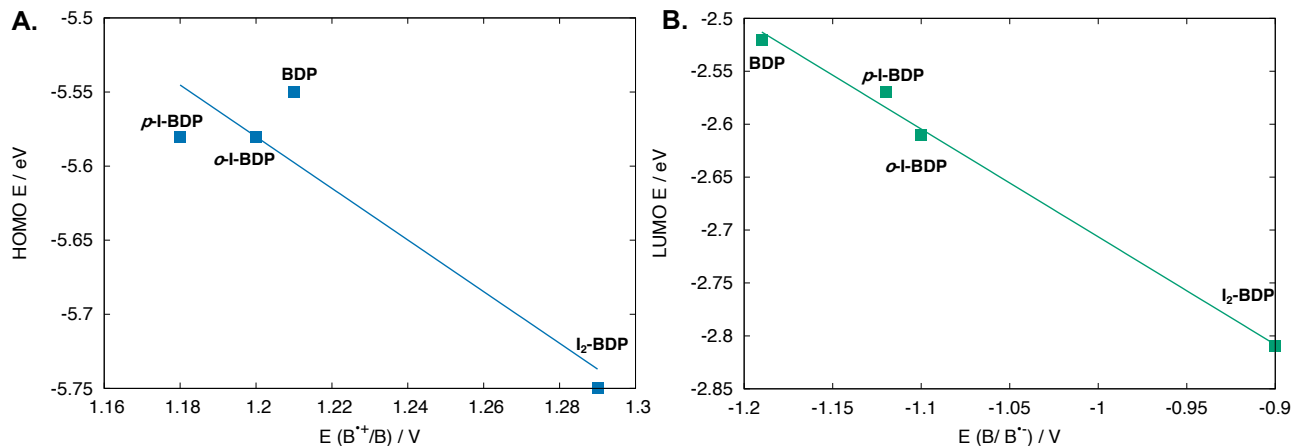
Figure 6. Relationship between (A) the $B^{·+}/B$ redox potentials (see table 2) and H energies; (B) the $B/B^{·−}$ redox potentials (see table 2) and L energies of BODIPY derivatives. H and L energies calculated at PCM-B3LYP/6-31G*/LANL2DZ level (see *Table S3*).

Accurate computational predictions of redox potentials require comparison of energies for both the starting molecule and its reduced/oxidized forms. However, we can qualitatively use Koopmans' theorem[30] to correlate the redox potentials of BODIPY derivatives with H/L computed energies. The result of such correlations is shown in *Figure 6A and 6B*, where a plot of the computed H/L energies versus experimental redox potentials shows good linearity especially for L energies. The fitting of H energies versus $B^{·+}/B$ redox potentials shows some deviations: **BDP**'s oxidation potential is slightly higher than those of **o-I-BDP** and **p-I-BDP**. It should be noted however that these differences are small and are within experimental uncertainties. Interestingly, both markedly different redox potentials of **I₂-BDP** are correctly captured by computations.

3.4.2 Low-lying excited states
To identify the deactivation pathways of the four BODIPY derivatives, we determined the most relevant excitation energies and excited state wavefunctions with PCM-TD-M06-2X/6-311G*/LANL2DZ calculations (including the standard LR description of solvent effects) at the PCM-B3LYP/6-31G*/LANL2DZ optimized ground state geometries (see *Table S4*). The corresponding molecular orbitals are depicted in *Figure S5*. As expected, the S_1 and T_1 states are dominated by the H→L excitation, localized on the BODIPY core. In addition to the lowest triplet state, in *Table S4* we also report the excitation energy of the second lowest triplet T_2, which is computed to be very close to S_1 and is also dominated by an excitation localized on the BODIPY core, for all the systems investigated.

The quality of predicted excited states can be assessed by comparing computed absorption spectra in solution with the experimental data. To this end, we determined the cLR(NEQ) corrected excitation energy of S_1 (see *Table S5*), the state responsible for the main absorption band of BODIPY derivatives. The comparison between computed and experimental spectra is shown in *Figure 7* where a shift of 0.45 eV was applied to computed excitation energies to account for the systematic overestimation of S_1 excitation energy at TDDFT level,[14–16] as described in Section 2.2. Interestingly, the spectral changes induced by different iodination are very well reproduced by the calculations.

It is instructive to analyze in more detail the results of different computational protocols for solvent corrections. Solvatochromism in absorption spectra is determined by the different dipole moment of ground and excited states. Calculations show that the dipole moment (see *Table S6*) is systematically lower in S_1 compared to the ground state, for all the BODIPY derivatives investigated. This implies that an inverted solvatochromism[31] should be observed, accompanied by a blue shift when moving from gas-phase (calculations in vacuo) to MeCN. In contrast (see *Table S5)*, $S_0 \rightarrow S_1$ excitation energies computed in MeCN with the LR approach, decrease compared to gas-phase, while the expected excitation energy increase is predicted only by cLR(NEQ) calculations. Consider, for example the S_1 excitation energy computed at 2.97 eV in vacuo for **BDP**, which unexpectedly decreases to 2.87 eV in MeCN (LR) and correctly increases to 2.99 eV in MeCN (cLR(NEQ)). As a result of the incorrect LR description, the correspondingly computed spectra are red shifted, in *Figure S7*, compared to those obtained including the cLR(NEQ) solvent correction. The overshooting of positive solvatochromism by the LR approach has been documented in previous work [18,32]. Here we underscore that, for BODIPY derivatives characterized by inverted solvatochromism, the inclusion of solvent correction at LR level, incorrectly predicts an excitation energy decrease and only cLR provides a physically sound description of gas-phase to solvent excitation energy changes.
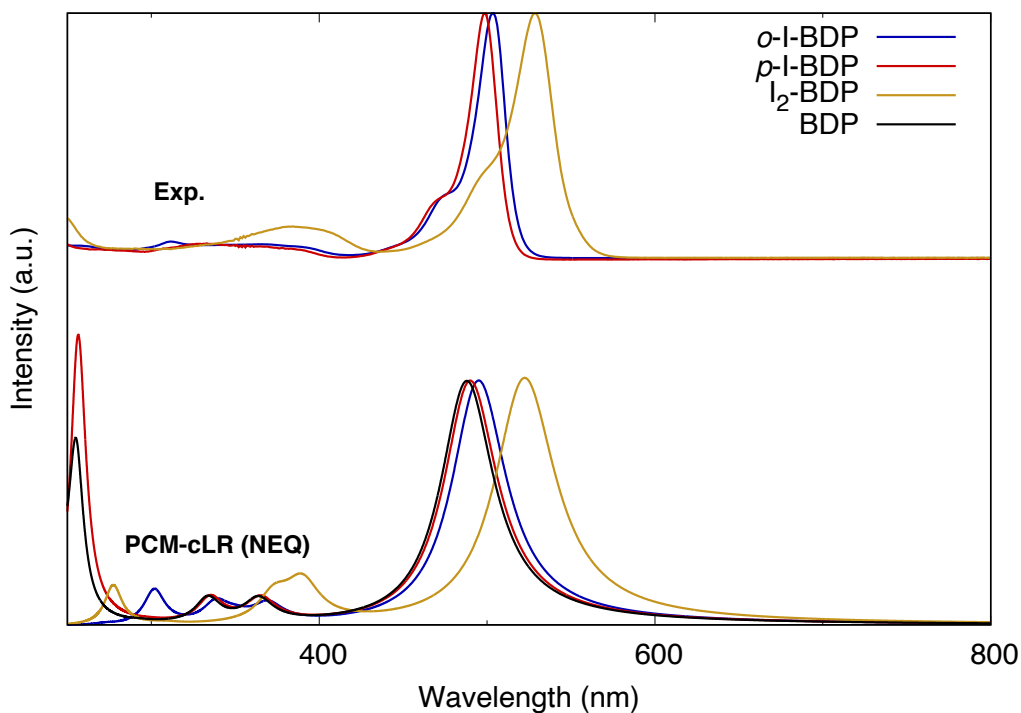

Figure 7. Comparison between computed and observed absorption spectra of the four investigated BODIPY derivatives. PCM-TD-M06-2X/6-311G* level of theory including cLR(NEQ) solvent corrections. The computed excitation energies were shifted by 0.45 eV in accordance with the known systematic overestimate at TDDFT level[15].

3.4.3 Predicted efficiency of ISC deactivation

Experimental data (*Table 1*) show that only *o*-**I-BDP** and **I₂-BDP** populate efficiently the lowest triplet state T_1 and exhibit relevant Φ_Δ values. Furthermore, the efficiency is greater for **I₂-BDP** with respect to *o*-**I-BDP** while population of T_1 is an inefficient process for *p*-**I-BDP** and **BDP.**

According to the excited state calculations discussed in the previous section, two triplet states lie below (T_1) or close (T_2) to S_1 and should be considered to rationalize the experimental results. Because the ISC process is relatively slow[33] (of the order of 10^7-10^8 s^{-1}) compared to typical timescales of solvent reorganization[34] (picosecond, sub-picosecond), we can safely assume that solvent equilibration occurs. Thus, solvent-equilibrated excited state energies (cLR(EQ)) (see *Figure 8*) are considered in the following discussion. As discussed above, the S_1 state (blue diamond, *Figure 8*) is found between T_1 and T_2 states, and quite close to the latter. Therefore, the $S_1 \rightarrow T_2$ ISC cannot be ruled out. Indeed, in recent investigations on different BODIPY derivatives[35,36] it has been proposed that the $S_1 \rightarrow T_2$ deactivation path can be a relevant ISC channel.
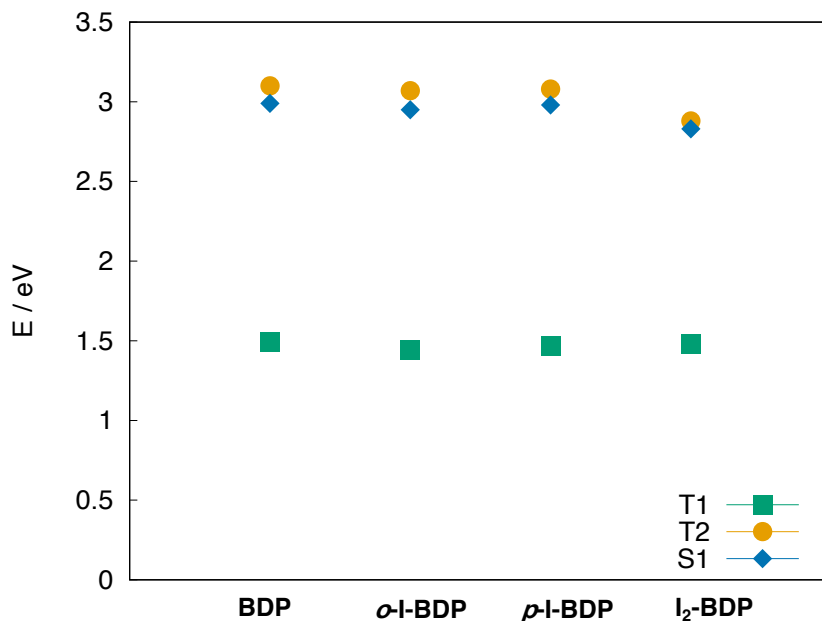

Figure 8. Computed excitation energies (PCM-TD-M06-2X/6-311G*/LANL2DZ level, including cLR(EQ) solvent correction) of low lying singlet and triplet excited states of **BDP** and iodinated derivatives.

For radiationless transitions slower than vibrational relaxation,[37] and for relatively large energy gaps ΔE_{S-T} between S_1/T_n states, the ISC process can be discussed in terms of a simplified relation (*Equation 2*), where the rate constant (k_{ISC}) is proportional to the SOC matrix element $\langle T_n|\widehat{H_{SO}}|S_1\rangle$ and inversely proportional to the square of the energy gap ΔE_{S-T} between S_1/T_n states[35,37–39]:

$$k_{ISC} \propto \frac{\left|\langle T_n|\widehat{H_{SO}}|S_1\rangle\right|^2}{(\Delta E_{S-T})^2}$$

$$(2)$$

The SOCs between T_1,T_2 and S_1, computed at the optimized PCM-B3LYP (PCM-M06-2X) geometries are collected in *Table 3* (*Table S7*). In the same table we also report the relevant ΔE_{S-T} values taken from cLR(EQ) calculations (*Fogure 8*, *Table S5*). Although the two sets of geometries display different degrees of orthogonality between the phenyl substituent and the BODIPY core and a different BF$_2$ out of plane tilt, it is interesting to note that both consistently suggest a similar decay pattern. The SOCs computed for the two geometries of *o*-**I-BDP** are very similar since this

is the only case in which the BODIPY derivative displays an orthogonal geometry also at PCM-M06-2X level. Concerning the magnitude of computed SOCs, we note that these are negligible for **BDP,** both at PCM-B3LYP and PCM-M06-2X geometries. For ***p*-I-BDP** the computed SOCs are also negligible for both sets of geometries, although slightly larger at the less symmetric PCM-M06-2X structure. A markedly different trend is documented for the remaining two iodinated derivatives. ***o*-I-BDP** displays, for both geometries, a relevant SOC between T_1 and S_1 and a non-negligible value between S_1 and T_2. It is well known that the presence of a second triplet state in the vicinity of the excited singlet greatly enhances the rate of the intersystem crossing.[40] Since ΔE_{S-T} is considerably smaller for the T_2 state, we cannot rule out a contribution from the $S_1 \rightarrow T_2$ ISC to the efficient triplet formation. Finally, very large SOCs are computed for **I$_2$-BDP** in perfect agreement with the remarkable effect experimentally documented for iodine atoms directly linked to the BODIPY core. While both SOCs between T_1 / S_1 and T_2 / S_1 are not negligible, we note that the less symmetric PCM-M06-2X structure leads to larger couplings and in particular the increase of $\langle T_1 | \widehat{H_{SO}} | S_1 \rangle$ is notable. At the same time the $\langle T_2 | \widehat{H_{SO}} | S_1 \rangle$ couplings are much larger than those computed for ***o*-I-BDP**. This, coupled to a reduction of the S_1/T_2 energy difference in **I$_2$-BDP**, points to an even more relevant role of the $S_1 \rightarrow T_2$ ISC for this system.

Thus, based on the above considerations, we expect negligible triplet generation for **BDP** and **p-I-BDP**. The most efficient triplet generation is predicted for **I$_2$-BDP** while an intermediate efficiency is expected for ***o*-I-BDP**. A possible additional deactivation pathway via $S_1 \rightarrow T_2$ ISC is predicted for both, with an increased efficiency for **I$_2$-BDP**. These conclusions are in agreement with experimental data.

Table 3. Computed spin-orbit couplings between S_1 and T_1/T_2 states of **BDP** and iodinated derivatives.

	SOC @geo PCM-B3LYP	
Molecule	S_1/T_1 [cm^{-1}][a] (ΔE_{S-T} [eV])[b]	S_1/T_2 [cm^{-1}][a] (ΔE_{S-T} [eV])[b]
***o*-I-BDP**	0.74 (1.51)	0.19 (-0.11)
***p*-I-BDP**	0.00 (1.51)	0.00 (-0.11)
I$_2$-BDP	0.52 (1.35)	8.62 (-0.05)
BDP	0.00 (1.50)	0.00 (-0.11)

[a] SOC values calculated with the SOMF(1X) approach, from TD-M06-2X/6-311G* calculations at PCM-B3LYP/6-31G* and PCM-B3LYP/6-31G*/LANL2DZ optimized geometries. [b] ΔE_{S-T} from PCM-TD-M06-2X/6-311G* and PCM-TD-M06-2X/6-311G*/LANL2DZ levels, including cLR(EQ) solvent correction.

4. Conclusions

The purpose of this work was the synthesis of fully-organic phosphorescent BODIPY derivatives. Given the improvements in the photophysical properties recently displayed by this class of molecules, the effort was aimed at the synthesis of BODIPYs that did not contain heavy metals but relied on iodine atoms for the efficient population of their triplet states. Monoiodination in the *ortho* position of *meso* phenyl-BODIPY, proved to be an effective way to gain access to the phosphorescent triplet state while maintaining fluorescent BODIPYs electrochemical properties. The molecules' photophysical and electrochemical properties are therefore decidedly influenced by the positions that iodine atoms occupy around the BODIPY core, and their rationalization was possible on the basis of the combined experimental and computational study.

Quantum chemical calculations were shown to support the remarkable changes in redox potentials of **I$_2$-BDP** and the relative shifts in absorption spectra along the series of BODIPY derivatives

investigated. From a methodological point of view, it was shown that only the cLR approach correctly describes solvatochromic effects in BODIPY derivatives, when moving from gas-phase to solvent. Finally, the computed low-lying excited states and SOCs were shown to be fully consistent with the inefficient triplet generation of **BDP** and *p*-**I-BDP**. The superior efficiency of **I$_2$-BDP** compared to *o*-**I-BDP** was demonstrated by large SOCs for the two available ISC pathways: S$_1$→T$_2$ and S$_1$→T$_1$. While functionalization of iodine atoms at different positions in **BDP** does not affect remarkably the nature of low-lying excited states, it modulates the relative energy of low-lying states. The tiny changes in wavefunctions induced by the presence and position of iodine atoms are nicely captured by the calculated SOCs which provide a consistent interpretation of the experimental data.

Conflicts of interest
The authors declare that they have no conflict of interest.

References
1   L. Y. Niu, H. Li, L. Feng, Y. S. Guan, Y. Z. Chen, C. F. Duan, L. Z. Wu, Y. F. Guan, C. H. Tung and Q. Z. Yang, BODIPY-based fluorometric sensor array for the highly sensitive identification of heavy-metal ions, *Anal. Chim. Acta*, 2013, **775**, 93–99.

2   T. Kowada and K. Kikuchi, BODIPY-based probes for the fluorescence imaging of biomolecules in living cells, *Chem. Soc. Rev.*, 2015, 4953–4972.

3   E. Bassan, A. Gualandi, P. G. Cozzi and P. Ceroni, Design of BODIPY dyes as triplet photosensitizers: electronic properties tailored for solar energy conversion, photoredox catalysis and photodynamic therapy, *Chem. Sci.*, 2021, **12**, 6607–6628.

4   T. Yogo, Y. Urano, Y. Ishitsuka, F. Maniwa and T. Nagano, Highly efficient and photostable photosensitizer based on BODIPY chromophore, *J. Am. Chem. Soc.*, 2005, **127**, 12162–12163.

5   V. Balzani, P. Ceroni and A. Juris, *Photochemistry and Photophysics. Concepts, Research, Applications*, Wiley, Weinheim, Germany, 2014.

6   A. Kamkaew, S. H. Lim, H. B. Lee, L. V. Kiew, L. Y. Chung and K. Burgess, BODIPY dyes in photodynamic therapy, *Chem. Soc. Rev.*, 2013, **42**, 77–88.

7   G. Magagnano, A. Gualandi, M. Marchini, L. Mengozzi, P. Ceroni and P. G. Cozzi, Photocatalytic ATRA reaction promoted by iodo-Bodipy and sodium ascorbate, *Chem. Commun.*, 2017, **53**, 1591–1594.

8   A. Boelke, E. Lork and B. J. Nachtsheim, N-Heterocycle-Stabilized Iodanes: From

Structure to Reactivity, *Chem. – A Eur. J.*, 2018, **24**, 18653–18657.

9   Y. Xu, D. Chang, S. Feng, C. Zhang and J. X. Jiang, BODIPY-containing porous organic polymers for gas adsorption, *New J. Chem.*, 2016, **40**, 9415–9423.

10   C. Zhang, J. Zhao, S. Wu, Z. Wang, W. Wu, J. Ma, S. Guo and L. Huang, Intramolecular RET enhanced visible light-absorbing bodipy organic triplet photosensitizers and application in photooxidation and triplet-triplet annihilation upconversion, *J. Am. Chem. Soc.*, 2013, **135**, 10566–10578.

11   L. Zoli and P. G. Cozzi, Electrophilic activation of aldehydes 'on water': A facile route to dipyrromethanes, *ChemSusChem*, 2009, **2**, 218–220.

12   W. R. Wadt and P. J. Hay, Ab initio effective core potentials for molecular calculations. Potentials for main group elements Na to Bi, *J. Chem. Phys.*, 1985, **82**, 284–298.

13   J. Tomasi, B. Mennucci and R. Cammi, Quantum mechanical continuum solvation models, *Chem. Rev.*, 2005, **105**, 2999–3093.

14   V. Postils, F. Ruipérez and D. Casanova, Mild Open-Shell Character of BODIPY and Its Impact on Singlet and Triplet Excitation Energies, *J. Chem. Theory Comput.*, 2021, **17**, 5825–5838.

15   F. Zinna, T. Bruhn, C. A. Guido, J. Ahrens, M. Bröring, L. Di Bari and G. Pescitelli, Circularly Polarized Luminescence from Axially Chiral BODIPY DYEmers: An Experimental and Computational Study, *Chem. Eur. J.*, 2016, **22**, 16089–16098.

16   S. Chibani, A. D. Laurent, B. Le Guennic and D. Jacquemin, Improving the accuracy of excited-state simulations of BODIPY and Aza-BODIPY dyes with a joint SOS-CIS(D) and TD-DFT approach, *J. Chem. Theory Comput.*, 2014, **10**, 4574–4582.

17   S. Chibani, B. Le Guennic, A. Charaf-Eddin, A. D. Laurent and D. Jacquemin, Revisiting the optical signatures of BODIPY with ab initio tools, *Chem. Sci.*, 2013, **4**, 1950–1963.

18   A. Charaf-Eddin, B. Le Guennic and D. Jacquemin, Excited-states of BODIPY-cyanines: Ultimate TD-DFT challenges?, *RSC Adv.*, 2014, **4**, 49449–49456.

19   M. Laine, N. A. Barbosa, R. Wieczorek, M. Y. Melnikov and A. Filarowski, Calculations of BODIPY dyes in the ground and excited states using the M06-2X and PBE0 functionals, *J. Mol. Model.*, 2016, **22**, 260.

20   B. Mennucci, Modeling absorption and fluorescence solvatochromism with QM/Classical approaches, *Int. J. Quantum Chem.*, 2015, **115**, 1202–1208.

21   M. Caricato, B. Mennucci, J. Tomasi, F. Ingrosso, R. Cammi, S. Corni and G. Scalmani, Formation and relaxation of excited states in solution: a new time dependent polarizable continuum model based on time dependent density functional theory., *J. Chem. Phys.*, 2006, **124**, 124520.

22   M. J. Frisch, G. W. Trucks, H. B. . Schlegel, G. E. Scuseria, M. A. Robb, J. R. Cheeseman,

G. . Scalmani, V. Barone, G. A. Petersson, H. Nakatsuji, X. . Li, M. Caricato, A. V. . Marenich, J. Bloino, B. G. Janesko, R. Gomperts, B. Mennucci, H. P. Hratchian, J. V. Ortiz, A. F. Izmaylov, J. L. Sonnenberg, D. Williams-Young, F. Ding, F. Lipparini, F. Egidi, J. Goings, B. Peng, A. Petrone, T. Henderson, D. . Ranasinghe, J. Zakrzewski, V. G.; Gao, N. Rega, G. Zheng, W. Liang, M. Hada, M. Ehara, K. . Toyota, R. Fukuda, J. Hasegawa, M. Ishida, T. . Nakajima, Y. . Honda, O. . Kitao, H. . Nakai, T. . Vreven, K. . Throssell, J. Montgomery, J. A., J. E. Peralta, F. Ogliaro, M. J. Bearpark, J. J. Heyd, E. N. Brothers, K. N. . Kudin, V. N. . Staroverov, T. A. Keith, R. Kobayashi, J. Normand, K. Raghavachari, A. P. Rendell, J. C. Burant, S. S. Iyengar, J. Tomasi, M. . Cossi, J. M. . Millam, M. . Klene, C. . Adamo, R. . Cammi, J. W. Ochterski, R. L. Martin, K. Morokuma, O. Farkas, J. B. Foresman and D. J. Fox, *Gaussian, Inc., Wallingford CT*, 2016.

23   F. Neese, F. Wennmohs, U. Becker and C. Riplinger, The ORCA quantum chemistry program package, *J. Chem. Phys.*, 2020, **152**, 224108.

24   B. De Souza, G. Farias, F. Neese and R. Izsák, Predicting Phosphorescence Rates of Light Organic Molecules Using Time-Dependent Density Functional Theory and the Path Integral Approach to Dynamics, *J. Chem. Theory Comput.*, 2019, **15**, 1896–1904.

25   F. Neese, Efficient and accurate approximations to the molecular spin-orbit coupling operator and their use in molecular g-tensor calculations, *J. Chem. Phys.*, 2005, **122**, 034107.

26   Y. Gabe, Y. Urano, K. Kikuchi, H. Kojima and T. Nagano, Highly Sensitive Fluorescence Probes for Nitric Oxide Based on Boron Dipyrromethene Chromophore - Rational Design of Potentially Useful Bioimaging Fluorescence Probe, *J. Am. Chem. Soc.*, 2004, **126**, 3357–3367.

27   N. Duvva, K. Sudhakar, D. Badgurjar, R. Chitta and L. Giribabu, Spacer controlled photo-induced intramolecular electron transfer in a series of phenothiazine-boron dipyrromethene donor–acceptor dyads, *J. Photochem. Photobiol. A*, 2015, **312**, 8–19.

28   W. Li, L. Li, H. Xiao, R. Qi, Y. Huang, Z. Xie, X. Jing and H. Zhang, Iodo-BODIPY: A visible-light-driven, highly efficient and photostable metal-free organic photocatalyst, *RSC Adv.*, 2013, **3**, 13417–13421.

29   Y. Mao, M. Head-Gordon and Y. Shao, Unraveling substituent effects on frontier orbitals of conjugated molecules using an absolutely localized molecular orbital based analysis, *Chem. Sci.*, 2018, **9**, 8598–8607.

30   T. Koopmans, Über die Zuordnung von Wellenfunktionen und Eigenwerten zu den Einzelnen Elektronen Eines Atoms, *Physica*, 1934, **1**, 104–113.

31   H. Sunahara, Y. Urano, H. Kojima and T. Nagano, Design and synthesis of a library of BODIPY-based environmental polarity sensors utilizing photoinduced electron-transfer-controlled fluorescence ON/OFF switching, *J. Am. Chem. Soc.*, 2007, **129**, 5597–5604.

32   S. Chibani, A. Charaf-Eddin, B. Le Guennic and D. Jacquemin, Boranil and Related NBO Dyes: Insights From Theory, *J. Chem. Theory Comput.*, 2013, **9**, 3127–3135.

33   J. T. Buck, A. M. Boudreau, A. DeCarmine, R. W. Wilson, J. Hampsey and T. Mani, Spin-Allowed Transitions Control the Formation of Triplet Excited States in Orthogonal Donor-Acceptor Dyads, *Chem*, 2019, **5**, 138–155.

34   S. Park, J. Kim, A. M. Moran and N. F. Scherer, Solvent structural relaxation dynamics in dipolar solvation studied by resonant pump polarizability response spectroscopy, *Phys. Chem. Chem. Phys.*, 2011, **13**, 214–223.

35   Y. Dong, P. Kumar, P. Maity, I. Kurganskii, S. Li, A. Elmali, J. Zhao, D. Escudero, H. Wu, A. Karatay, O. F. Mohammed and M. Fedin, Twisted BODIPY derivative: intersystem crossing, electron spin polarization and application as a novel photodynamic therapy reagent, *Phys. Chem. Chem. Phys.*, 2021, **23**, 8641–8652.

36   R. R. Valiev, V. N. Cherepanov, G. V. Baryshnikov and D. Sundholm, First-principles method for calculating the rate constants of internal-conversion and intersystem-crossing transitions, *Phys. Chem. Chem. Phys.*, 2018, **20**, 6121–6133.

37   V. G. Plotnikov, Regularities of the processes of radiationless conversion in polyatomic molecules, *Int. J. Quantum Chem.*, 1979, **16**, 527–541.

38   Y.-L. Chen, S.-W. Li, Y. Chi, Y.-M. Cheng, S.-C. Pu, Y.-S. Yeh and P.-T. Chou, Switching Luminescent Properties in Osmium-Based β-Diketonate Complexes, *ChemPhysChem*, 2005, **6**, 2012–2017.

39   J. Zhang, S. Mukamel and J. Jiang, Aggregation-Induced Intersystem Crossing: Rational Design for Phosphorescence Manipulation, *J. Phys. Chem. B*, 2020, **124**, 2238–2244.

40   M. Bixon and J. Jortner, Intramolecular Radiationless Transitions, *J. Chem. Phys.*, 1968, **48**, 715–726.